

# The glacial express

Kevin G. Harrison<sup>1\*</sup>

This paper is a non-peer reviewed preprint submitted to EarthArXiv.

May 28, 2019

<sup>1</sup>Geosciences Department, Denison University, 100 West College Street, Granville, OH 43023-0810 USA.

\*harrisonk@denison.edu, 740-587-4898, Orcid ID# 0000-0002-6921-7203.

**Glacial calcium carbonate (CaCO<sub>3</sub>) shells are larger than interglacial CaCO<sub>3</sub> shells<sup>1-5</sup>. My research explores the consequences of this size difference. Because larger CaCO<sub>3</sub> shells sink faster<sup>6,7</sup> and dissolve more slowly<sup>8</sup> than smaller CaCO<sub>3</sub> shells, larger glacial shells underwent less dissolution than smaller interglacial shells. The resulting CaCO<sub>3</sub> transport efficiency increase, coupled with observations that CaCO<sub>3</sub> delivery to deep-ocean sediments remained about the same between glacial and interglacial times<sup>9-12</sup>, implies that glacial production of CaCO<sub>3</sub> in the mixed layer decreased by ~45%. This decrease helps explain why CO<sub>2</sub> levels were lower and why atmospheric radiocarbon levels were higher during glacial times. This research also explores the decrease in CaCO<sub>3</sub> transport efficiency caused by ocean acidification. Furthermore, it explains how large CaCO<sub>3</sub> shells can form in high-energy environments at high pCO<sub>2</sub> levels.**

## Introduction

During glacial times, CaCO<sub>3</sub> shells produced by plankton had more mass than CaCO<sub>3</sub> shells produced by plankton during interglacial times (Table 1). For example, during the last glacial maximum (LGM), the mass of *E. Huxleyi* coccoliths averaged 5.2 pg, but their mass decreased to 4.3 pg a few thousand years ago<sup>1</sup>. Further, the average coccolith mass during the LGM was 12 pg, but mass decreased to 9 pg more recently<sup>1</sup>. Because average mass change includes shifts in species abundance that tend to favor larger species during glacial times<sup>1</sup>, average mass change is a better indicator of shifts in coccolithosphere size for a specific species. My research explores reasons why CaCO<sub>3</sub> shells produced during glacial times had more mass than their interglacial counterparts and discusses how this mass increase influenced global biogeochemical cycles and the marine sedimentary record. For example, heavier glacial shells sink faster than their lighter interglacial counterparts, increasing the efficiency of CaCO<sub>3</sub> delivery to the deep ocean. In addition to sinking faster, larger CaCO<sub>3</sub> shells dissolve more slowly than smaller shells, further increasing the efficiency of CaCO<sub>3</sub> delivery to the deep ocean.

## Differences between glacial and interglacial CaCO<sub>3</sub> planktonic shells

Several researchers have found that CaCO<sub>3</sub> shells produced by plankton were larger during glacial times than in interglacial times (Table 1). pCO<sub>2</sub> levels were low during the LGM and increased during interglacial times. Both coccolithophores (phytoplankton) and forams (zooplankton) produced larger CaCO<sub>3</sub> shells during glacial times.

*Coccolithophores*

Coccolithophores produce most of the open-ocean CaCO<sub>3</sub> (13). Coccolithophores are plankton that produce CaCO<sub>3</sub> coccoliths, which resemble plates or shields, and combine to form spheres (coccospheres).

Beaufort et al. created a 40,000-year record that documents how coccolith shells respond to changing CO<sub>2</sub> levels<sup>1</sup>. They collected 180 surface water samples and 555 sediment-core samples to study the effects of carbonate chemistry and other environmental factors on coccolithophores. Each sample had an average of 700 coccoliths. They found that coccolith mass correlated with coccosphere mass ( $R^2 = 0.88$ ) and that coccolith mass decreased when pCO<sub>2</sub> increased. During the LGM, from ~17 to ~24 ky, *E. Huxleyi* coccoliths weighed ~5.2 pg (1, their Fig. 2b). During interglacial times, *E. Huxleyi* coccoliths weighed ~4.3 pg from ~0 to ~5 ky, about an 18% decrease in mass. The coccolith masses for *G. Oceanica* decreased from an LGM value of 24.5 pg to a Holocene value of 21 pg (1, their Fig. 1c). During the LGM, *G. Oceanica* coccoliths weighed about 17% more, on average, than Holocene *G. Oceanica* coccoliths.

Plankton species with large CaCO<sub>3</sub> shells (e.g., *G. Oceanica*) were more abundant than plankton species with small CaCO<sub>3</sub> shells (*E. huxleyi*) when atmospheric CO<sub>2</sub> levels were low. Beaufort et al. found that the abundance of *G. Oceanica* relative to *E. huxleyi* increased by ~25% during glacial times in low latitudes compared to interglacial times in low latitudes<sup>1</sup>.

The shift in CaCO<sub>3</sub> shell mass may have been due to both an increase in shell mass within species and an increase in the abundance of species with larger shells. For example, the average coccolith mass was ~12 pg when pCO<sub>2</sub> was ~196 ppm, while the mass decreased to about 9 pg when pCO<sub>2</sub> was ~280 ppm (1, their Fig. 1c). For this study, a value of 33% mass increase during the LGM is used, because it reflects both the increase in size within a species and the increase in abundance of larger species of plankton with CaCO<sub>3</sub> shells (Table 1). Since this research could find no evidence of large changes in CaCO<sub>3</sub> density between glacial and interglacial times, it translates the observed 33% increase in CaCO<sub>3</sub> shell mass into a 33% increase in CaCO<sub>3</sub> shell size.

Henderiks and Renaud<sup>2</sup> (see their Table 2) found that coccolith size for *C. Leptoporus* varied between glacial and interglacial times in offshore low-energy environments (Tables 1 and 2). For example, the average interglacial size was  $6.92 \pm 1.36 \mu\text{m}$  for core N3KF21,  $6.24 \pm 1.02 \mu\text{m}$  for core T88-9P, and  $6.78 \pm 1.05 \mu\text{m}$  for core 4242-01. The average of these three interglacial cores is  $6.65 \pm 0.36 \mu\text{m}$ . In contrast, the glacial size was  $7.43 \pm 1.79 \mu\text{m}$  for core 4242-03 and  $7.50 \pm 1.52 \mu\text{m}$  for core 4241-43. The average of these two glacial cores is  $7.47 \pm 0.05 \mu\text{m}$ . *C. Leptoporus* were 12% larger during glacial times. They observed the same trend for nearshore high-energy environments (Table 2).

### Forams

Forams and coccoliths produce most of the pelagic carbonate<sup>3</sup>. Barker and Elderfield<sup>4</sup> (data obtained from their Fig. 2) found that during glacial times, *G. bulloides* (300-355  $\mu\text{m}$  size fraction from core NEAP 8K) weighed 18  $\mu\text{g}$  during the LGM (17-24 ky), compared to the 12  $\mu\text{g}$  weight of their interglacial (0-5 ky) counterparts (Table 1). Forams in this core weighed 50% more during glacial times.

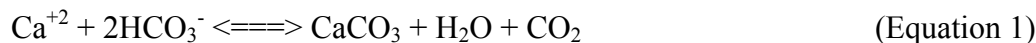
Moy et al.<sup>5</sup> collected *G. bulloides* shells (300-355  $\mu\text{m}$  size fraction) in core GC17. Shells collected during the LGM (18-24 kyr) had an average weight of 30.3  $\mu\text{g}$  (Table 1). In contrast, Holocene (0-10 ky) shells had an average weight of 24.4  $\mu\text{g}$  (Table 1). Glacial foram shells weighed about 24% more than their interglacial counterparts in core GC17.

### Implications

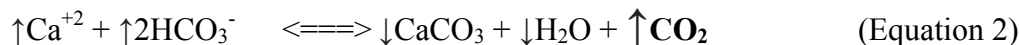
Larger  $\text{CaCO}_3$  shells may cause ecological and biogeochemical changes. For example, Monteiro et al.<sup>6</sup> suggest that thicker coccolithospheres protect against predation. Also, larger  $\text{CaCO}_3$  shells that formed during the LGM may be more efficient at ballasting organic material, which then increases the effectiveness of the organic tissue pump. Larger shells may increase survival in high-energy environments. More importantly, the consequences resulting from increased  $\text{CaCO}_3$  transport efficiency associated with increased shell size may help explain several glacial puzzles, including why  $\text{CO}_2$  levels were lower during glacial times.

### Influence of $\text{pCO}_2$ on shell formation

According to Le Chatelier's principle, adding reactants to a chemical reaction will increase the formation of products, while adding products will increase the formation of reactants. Consider the equation for the formation of  $\text{CaCO}_3$ :

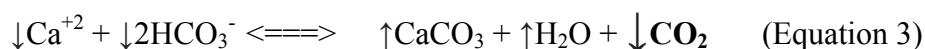


Dissolved calcium ( $\text{Ca}^{+2}$ ) combines with bicarbonate ( $\text{HCO}_3^-$ ) to form calcium carbonate or calcite ( $\text{CaCO}_3$ ), carbon dioxide ( $\text{CO}_2$ ) and water ( $\text{H}_2\text{O}$ ). According to Le Chatelier's principle, adding  $\text{CO}_2$ , a product, to the steady-state system will shift the  $\text{CaCO}_3$  reaction to the left (favoring reactants) and dissolve  $\text{CaCO}_3$  (removing products):



Adding  $\text{CO}_2$  ( $\uparrow\text{CO}_2$ ) will decrease  $\text{CaCO}_3$  ( $\downarrow\text{CaCO}_3$ ) and  $\text{H}_2\text{O}$  ( $\downarrow\text{H}_2\text{O}$ ) concentrations and increase  $\text{Ca}^{+2}$  ( $\uparrow\text{Ca}^{+2}$ ) and  $\text{HCO}_3^-$  ( $\uparrow 2\text{HCO}_3^-$ ) concentrations. This represents ocean acidification, which has been observed in the contemporary ocean and linked to the build-up of atmospheric  $\text{CO}_2$  levels<sup>14,15</sup>.

In contrast, removing  $\text{CO}_2$  will shift the reaction to favor the reactants and create  $\text{CaCO}_3$ . This may have occurred during the LGM, when  $\text{CO}_2$  levels were low. In short, Le Chatelier's principle predicts that decreasing  $\text{CO}_2$  levels will increase calcification rates, which may increase size and mass of  $\text{CaCO}_3$  shells.



Predictions of changes in  $\text{CaCO}_3$  shell mass in response to changing  $\text{pCO}_2$  levels based on Le Chatelier's principle have been supported by observations. For example, Beaufort et al.<sup>1</sup> found that carbonate chemistry determined the coccosphere mass in their 40,000-year record.

Specifically, they discovered that the  $\text{CaCO}_3$  mass depended on carbonate concentration [ $\text{CO}_3^{-2}$ ] and the  $\text{CaCO}_3$  saturation state [ $\Omega\text{Ca}$ ] ( $R^2 = 0.74$ ). Since  $\text{pCO}_2$  and [ $\text{CO}_3^{-2}$ ] vary inversely,

surface pCO<sub>2</sub> may influence the size of coccospheres. Surprisingly, Beaufort et al. found that temperature, salinity, light, and nutrients were not strongly correlated with coccolith mass<sup>1</sup>. They also concluded that the mass of coccoliths serves as a proxy for calcification state.

Beaufort et al. found that coccolith mass increased with increasing carbonate<sup>1</sup>. For example, at 100 μmol/kg of [CO<sub>3</sub><sup>-2</sup>], the average coccolith mass was ~4 pg; at 300 μmol/kg [CO<sub>3</sub><sup>-2</sup>], the average coccolith mass was ~12 pg. Increasing the carbonate concentration by a factor of three increased coccolith mass by about a factor of three. CaCO<sub>3</sub> shell dissolution occurs primarily in the water column at depths where CaCO<sub>3</sub> is undersaturated, such as the CaCO<sub>3</sub> transition zone.

### **CaCO<sub>3</sub> size and high-energy environments**

High-energy environments may cause thicker, more robust, or larger shells to form. High-energy environments are characterized by fast currents, frequent storms, or large waves. They include coastal areas and upwelling zones. For example, Akester and Martel found that bay mussels (*Mytilus Trossulus*) had thicker shells in wave-exposed habitats compared to wave-sheltered habitats<sup>16</sup>. High-energy environments may favor coccolithophores and forams with larger shells.

Smith et al. found that “heavily-calcified” *E. Huxleyi* morphotype abundance was >90% in the winter when pH and CaCO<sub>3</sub> saturation were the lowest<sup>17</sup>. In summer, the abundance of the heavily-calcified *E. Huxleyi* morphotype was <10%, even though pH and CaCO<sub>3</sub> saturation were higher. One expects heavily-calcified coccolithophores to be more abundant in the summer, due to the lower pH and CaCO<sub>3</sub> saturation. Perhaps, the heavily-calcified morphotypes are more dominant in the winter because winter storms in the Bay of Biscay create a high-energy environment that favors heavily-calcified coccolithophores. Table 3 shows seasonal variations in storms and heavily-calcified *E. Huxleyi* morphotype abundance. February and December were the months with the highest abundance of heavily-calcified morphotypes and were the months with the most gales.

Beaufort et al. collected coccospheres that formed in low-energy and high-energy environments: At low-energy station ST18, coccospheres were collected ~1000 km off the coast of Chile<sup>1</sup>. They found that <10% of these coccospheres had diameters that exceeded 6.6 μm. The low abundance of large coccospheres may reflect their low-energy environment. In contrast, station UPX was located in the Chile upwelling region, a high-energy environment. >60% of the UPX coccospheres were larger than 6.6 μm. The relatively high abundance of large coccospheres at the UPX site may reflect their high-energy environment.

Henderiks and Renaud<sup>2</sup> studied the coccolith size for *C. Leptoporus* in high-energy environments (nearshore) during the Holocene and the LGM (Table 2). The size of Holocene *C. Leptoporus* shells was 7.28 ± 1.48 μm for core 5559-03, 7.35 ± 1.31 μm for core 4216-02, and 7.25 ± 1.55 μm for core V23-98. The average value for these three cores is 7.29 ± 0.05 μm, which is 10% larger than their low-energy Holocene counterparts. These sizes increased during the LGM: 8.86 ± 1.77 μm from core 5559-48, 8.27 ± 1.51 μm for core 4216-73, and 7.22 ± 1.65 μm for core 1048-78. The average value is 8.12 ± 0.83 μm, which is 8% larger than their low-energy glacial counterparts.

pCO<sub>2</sub> appears to have a greater impact than energy levels on coccolith shell size (Table 2): The coccoliths that formed in low-energy environments during the LGM had an average size of 7.47 μm. The coccoliths that formed in high energy environments during the Holocene had an average size of 7.29 μm. The low-pCO<sub>2</sub>, low-energy coccoliths were 2.4% larger than the high-pCO<sub>2</sub>, high-energy coccoliths. This suggests that Holocene CaCO<sub>3</sub> shells formed by plankton may serve as surrogates for planktonic CaCO<sub>3</sub> shells formed during the LGM. Further, because CaCO<sub>3</sub> shell mass depends on pCO<sub>2</sub> and the energy level in the ocean environment where the shell grew, CaCO<sub>3</sub> shell mass may not be a reliable index for carbonate concentration in the deep ocean.

### **Glacial Express**

The bulk of CaCO<sub>3</sub> dissolution occurs in the water column<sup>8</sup>. Most CaCO<sub>3</sub> shell dissolution also occurs in water that is undersaturated in CaCO<sub>3</sub>. When CaCO<sub>3</sub> shells reach the sediments, their dissolution rates slow dramatically<sup>8</sup>. Ramisch et al. found that particle size and settling time were the two most important factors in determining CaCO<sub>3</sub> retention in sediments in lakes<sup>18</sup>. They found that CaCO<sub>3</sub> particles with diameters smaller than 41 μm never survived past a depth of 288 meters. If a particle is too small, it will dissolve before reaching the sediments. Larger particles will also undergo dissolution, but a portion will survive. Their findings may extend to oceans. The amount of dissolution that occurs in the water column depends on the sinking velocity and the dissolution rate of the shell, which both depend on the size of the shell. As shown below, large particles sink faster than small particles, so large CaCO<sub>3</sub> shells produced during the LGM may have sunk faster than their smaller Holocene counterparts, increasing the efficiency of CaCO<sub>3</sub> transport.

### **Velocity estimates: consider a spherical shell**

The velocities of different-sized particles are compared here using Stokes' Law. These theoretical calculations illustrate how particle size may influence the sinking velocities of CaCO<sub>3</sub> shells. The limitations of the Stokes' Law estimates for this research are addressed in the "Discussion" section.

The velocities of sinking particles in the ocean can be estimated using Stokes' Law (Equation 4). This is a first-order approximation, because factors such as upwelling can significantly alter sinking rates and because shells are not perfect spheres. Two key parameters that influence the rate of sinking are the diameter and density of the sphere:

*Stokes' Law*

$$V_t = gd^2(p_p - p_m)/(18u) \quad (\text{Equation 4})$$

V<sub>t</sub> is the terminal velocity, g is the acceleration due to gravity, d is the particle diameter, p<sub>p</sub> is the particle density, p<sub>m</sub> is the density of seawater, and u is the dynamic viscosity of seawater.

*Calculating the density and viscosity of seawater: interglacial and glacial*

The density and dynamic viscosity of seawater can be calculated using temperature, salinity and pressure<sup>19,20</sup> (Table 4). The average Holocene ocean temperature was 3.5° C, while the average temperature during the LGM was 0.9° C (21). The interglacial salinity of the ocean was 34.7‰,

while the salinity was 35.9‰ during the LGM<sup>22</sup>. The density of CaCO<sub>3</sub> shells is ~1.2 g/ml (23,24).

Fig. 1 shows the relationship between diameter and sinking velocity in the ocean during the LGM and Holocene:

$$\text{LGM Velocity} = 0.017882 * (\text{shell diameter})^{2.0026} \quad (\text{Equation 5})$$

$$\text{Holocene Velocity} = 0.019965 * (\text{shell diameter})^{1.9996} \quad (\text{Equation 6})$$

Velocity units are cm/hr and the diameter units are μm.

This work defines a Stokes' Law Shell as a hypothetical shell that follows Stokes' Law. A 10-μm Stokes' Law Shell would sink at a rate of 1.83 cm/hr during the Holocene (shell density = 1.2 g/ml, salinity = 34.7, temperature = 3.5° C, and pressure = 400 bar), while the same shell would sink at a rate of 1.67 cm/hr during the LGM (shell density = 1.2 g/ml, salinity = 35.9, temperature = 0.9, and pressure = 400 bar). The shell sinks more slowly during the LGM because the seawater has a higher density and dynamic viscosity (Table 4).

Table 4 illustrates how a Stokes' Law Shell differs between the Holocene and LGM. During the LGM, the Stokes' Law Shell would be 33% larger, on average, as discussed above. Hence, a 6 μm Holocene shell would be 8 μm in the LGM. The larger shell would sink ~62% faster, greatly increasing the efficiency of CaCO<sub>3</sub> transport to the deep ocean.

### Particle size and dissolution rate

Increasing the size of a sphere will decrease its dissolution rate, because when the diameter of a sphere increases, the volume increases more than the surface area: A sphere with a 250-μm diameter has a surface area of  $1.96 \times 10^5$  square μm and a volume of  $8.18 \times 10^6$  cubic μm. A sphere with a 333-μm diameter (i.e., a 33% larger diameter) will have a surface area of  $3.49 \times 10^5$  square μm (an increase of 78%) and a volume of  $1.94 \times 10^7$  cubic μm (an increase of 137%). This back-of-the-envelope prediction that larger shells will dissolve more slowly than smaller shells is supported by observations. For example, Morse found that CaCO<sub>3</sub> shells larger than 62 μm had a dissolution rate per unit area that was less than particles smaller than 62 μm (25). Also, Keir<sup>8</sup> measured the relationship between CaCO<sub>3</sub> shell dissolution rate and shell size (Fig. 2). Fitting a curve to Keir's data leads to Equation 7, which relates dissolution rate in percent dissolution per day to diameter in μm:

$$\text{Dissolution Rate} = 27392 * (\text{diameter})^{-1.1631} \quad (\text{Equation 7})$$

For example, a foram having a diameter of 250 μm, would have a CaCO<sub>3</sub> dissolution rate of 44.52%/day. A foram have a CaCO<sub>3</sub> shell that had a 33% larger diameter (e.g., 333 μm) would have a dissolution rate of 31.89%/day, which is 28% slower. This 28% decrease would apply to any 33% increase in size.

### Shell size and CaCO<sub>3</sub> transport efficiency

CaCO<sub>3</sub> shells produced during the LGM were about ~33% larger than their Holocene counterparts (Table 1). If these shells have sinking velocities that resemble the sinking velocities of Stokes' Law Shells, LGM shells will sink ~62% faster than Holocene shells. The validity of this assumption is discussed below. Also, the larger shells dissolve ~28% more slowly than their Holocene counterparts. Since most of CaCO<sub>3</sub> shell dissolution occurs in the water column<sup>8</sup>, the combined effects of the changes in sinking rate and dissolution rate imply that the CaCO<sub>3</sub> transport rate in the deep ocean will increase by ~90%.

CaCO<sub>3</sub> transport efficiency = shell sinking rate change – dissolution rate change (Equation 8)

### **Whole ocean CaCO<sub>3</sub> preservation: implications for surface ocean CaCO<sub>3</sub> production**

Because the efficiency of CaCO<sub>3</sub> transport to the deep ocean increased by ~90%, one expects the flux of CaCO<sub>3</sub> to the deep ocean to have also increased. An increase was not observed: Kohfeld et al. concluded that increases in deep-water carbonate-ion content and increases in CaCO<sub>3</sub> preservation were not observed during the LGM<sup>9</sup>; Catubig et al. estimated that Holocene CaCO<sub>3</sub> accumulation rates were  $8.3 \times 10^{12}$  moles/year<sup>10</sup>, while LGM CaCO<sub>3</sub> accumulation rates were  $9.2 \times 10^{12}$  moles/year (i.e., about the same, given the uncertainties of their method); Anderson and Archer concluded that there was little difference in foram preservation rates in marine sediments between the Holocene and the LGM<sup>11</sup>; and Farrell and Prell observed that the calcium critical depth (CCrD) remained constant between interglacial and glacial times<sup>12</sup>. (CCrD is the depth where ocean sediments contain 10% CaCO<sub>3</sub>.) In short, the flux of CaCO<sub>3</sub> to the deep ocean was about the same between glacial and interglacial times.

Since the CaCO<sub>3</sub> transport efficiency increased by ~90% and the CaCO<sub>3</sub> flux to the deep ocean remained constant, the production of CaCO<sub>3</sub> in the surface ocean must have decreased by ~45%. Decreasing surface ocean CaCO<sub>3</sub> production during the LGM would lower atmospheric carbon dioxide levels. Atmospheric CO<sub>2</sub> levels were lower during the LGM than during the Holocene (Table 5).

### **Atmospheric carbon dioxide levels**

During the LGM, atmospheric CO<sub>2</sub> levels were ~196 ppm and these levels increased to ~280 ppm in the Holocene (Table 5): During the LGM-to-Holocene transition, the size of the terrestrial biosphere increased, causing CO<sub>2</sub> levels to drop by 22 ppm. The increase in ocean temperature caused CO<sub>2</sub> levels to increase by 26 ppm. The decrease in ocean salinity caused CO<sub>2</sub> levels to decrease by 13 ppm. The net result of these changes decreased atmospheric CO<sub>2</sub> levels to 187 ppm.

Other mechanisms could increase atmospheric CO<sub>2</sub> levels. For example, Archer and Maier-Reimer concluded that increasing the flux of CaCO<sub>3</sub> to the deep ocean by 40% would increase atmospheric CO<sub>2</sub> levels by 84 ppm (26). A linear extrapolation of these results suggests that a 45% increase in surface CaCO<sub>3</sub> production would increase atmospheric CO<sub>2</sub> levels by 95 ppm (Table 5). This would bring the CO<sub>2</sub> level up from 187 ppm to 282 ppm, close to the observed value of 280 ppm (Table 5).

### **Atmospheric radiocarbon levels**

During the LGM, atmospheric radiocarbon levels ranged from +350‰ to +400‰, and they decreased to 0‰ in the Holocene<sup>27</sup>. Table 6 summarizes the processes that changed atmospheric radiocarbon levels during the LGM-to-Holocene transition: increased mass of the terrestrial biosphere, increased ocean ventilation rate, and increased CaCO<sub>3</sub> production in the surface ocean. Hughen et al. estimate that the increase in mass of the terrestrial biosphere would lower atmospheric radiocarbon levels by 10 to 30‰ and that increasing the ocean ventilation rate would lower atmospheric radiocarbon levels by 100 to 200‰ (27). Increasing the production of CaCO<sub>3</sub> in the surface ocean will lower atmospheric radiocarbon levels, because the flux of radiocarbon in CaCO<sub>3</sub> shells to the deep ocean decreases. Hughen et al. estimate that a 50% increase in surface CaCO<sub>3</sub> production would cause a 150‰ decrease in atmospheric radiocarbon<sup>27</sup>. A linear extrapolation of these results suggests that a 45% increase in surface CaCO<sub>3</sub> production would cause a 135‰ decrease in atmospheric radiocarbon (Table 6). The remaining 35 to 105‰ decrease could be caused by changes in the organic tissue pump or by iron fertilization.

### **Mechanisms for decreasing CaCO<sub>3</sub> production in the surface ocean during glacial times**

Coccolithophores and forams produce most of the CaCO<sub>3</sub> in the pelagic surface ocean<sup>3</sup>. If all of the CaCO<sub>3</sub> is produced by coccolithophores, then a 45% reduction in coccolithophore production would decrease total production by the same amount. If coccolithophores produce only 50% of the surface ocean CaCO<sub>3</sub> production, it would require a 90% reduction in coccolithophore production to cut total surface ocean CaCO<sub>3</sub> production by 45%. Coccolithophores make the bulk of the pelagic CaCO<sub>3</sub> (13).

There are at least two mechanisms that could have decreased coccolithophore production of CaCO<sub>3</sub> during glacial times: the silica hypothesis<sup>28,29</sup> and the silica-leakage hypothesis<sup>30</sup>.

#### *Silica hypothesis*

Harrison found that coccolithophore populations could be reduced enough to decrease atmospheric CO<sub>2</sub> from Holocene levels to LGM levels by increasing the supply of Si to the ocean<sup>28,29</sup>. One possible way to increase the Si supply to the ocean is by increasing the flux of dust to the mixed layer. Observations suggest that dust levels were higher during glacial times and that some of the Si present in dust dissolved and became available for biological uptake. Diatom populations increased at the expense of coccolithophores when the flux of Si to the mixed layer increased, because diatoms can outcompete coccolithophores.

#### *Silica-leakage hypothesis*

Matsumoto et al. concluded that increasing the flux of Fe to the mixed layer could decrease atmospheric carbon dioxide levels from 277 ppm to 230-242 ppm<sup>30</sup>. Like the silica hypothesis, the silica-leakage hypothesis is based on the increase in dust observed during glacial times and the ability of diatoms to outcompete coccolithophores. In short, some of the Fe present in dust becomes available for biological uptake. Hutchins and Bruland<sup>31</sup> and Takeda<sup>32</sup> found that increased Fe availability increased the C-to-Si ratio. Hence, diatom populations can increase with an increase in Fe. Further, Brzezinski et al. found that Fe and Si co-limit diatom production<sup>33</sup>.

#### *Implications*



The different characteristics of diatom shells during glacial times, such as the higher C/Si ratio, influence biogeochemical cycles that involve diatoms. If the diatom shells dissolve at shallower depths, the residence time for Si may have been faster during glacial times. Also, diatoms with higher C/Si ratios may have been less effective at ballasting organic carbon, decreasing the effectiveness of the organic tissue pump. Glacial diatom shells are less robust and less likely to have been preserved in marine sediments due to their thinner shells, which makes quantifying changes in diatom abundance between glacial and interglacial times difficult. The silica hypothesis and the silica-leakage hypothesis mechanisms may have worked in concert during glacial times.

### **Testing the “glacial-express” hypothesis**

The “glacial express” hypothesis, which says  $\text{CaCO}_3$  transport efficiency was greater during glacial times, can be tested by seeing how the  $\text{CaCO}_3$  dissolution zone changes between glacial and interglacial climates. Farrell and Prell defined the top of the  $\text{CaCO}_3$  transition zone as the depth where the  $\text{CaCO}_3$  concentration in sediments is 80% (12). They defined the bottom of the transition zone or Calcium Critical Depth (CCrD) as the depth where the sediments contain 10%  $\text{CaCO}_3$ . The  $\text{CaCO}_3$  transition zone reflects both the thermodynamics and kinetics of  $\text{CaCO}_3$  dissolution. During glacial maxima, one expects a thin transition zone, because  $\text{CaCO}_3$  transport is more efficient and causes abrupt dissolution gradients. Farrell and Prell observed an average thickness for the glacial transition zone of 230 meters for the past 800,000 years<sup>12</sup>. During interglacial times, one expects thick  $\text{CaCO}_3$  transition zones because  $\text{CaCO}_3$  transport is less efficient, which causes gradual dissolution gradients. Farrell and Prell observed an average thickness for the interglacial transition zone of 650 meters for the past 800,000 years<sup>12</sup>. In short, the glacial-express hypothesis is consistent with the changes in  $\text{CaCO}_3$  transition zone thickness observed by Farrell and Prell<sup>12</sup>: thinner transition zones during glacial maxima and thicker transition zones during interglacial times. Changes in sea level may alter the depth of the 80%  $\text{CaCO}_3$  level and the CCrD by about 130 meters between the Holocene and the LGM. However, the thickness of the  $\text{CaCO}_3$  transition zone should not be altered significantly by changes in sea level.

### **Future $\text{CaCO}_3$ transport by smaller shells in a warmer, less-saline ocean**

As contemporary atmospheric  $\text{CO}_2$  levels increase, the ocean becomes more acidic, warmer and less saline. Ocean acidification may decrease the size of  $\text{CaCO}_3$  shells by 33%, may warm the ocean by 2.6° C, and may decrease the salinity by 1.2‰ (Table 7). These differences are the same as differences found between the Holocene and the LGM. They illustrate how increased acidity, increased temperature and decreased salinity may impact  $\text{CaCO}_3$  transport efficiency in the future. These hypothetical changes in acidity, temperature, and salinity are not predictions and are only illustrative.

Table 7 shows how decreased shell size, increased temperature, and decreased salinity change the velocity of Stokes’ Law Shells. The densities are calculated at a pressure of 400 bar, which is close to the pressure near the top of the  $\text{CaCO}_3$  transition zone. The interglacial Stokes’ Law Shell velocity for a 6  $\mu\text{m}$  shell is ~0.64 cm/hr. Reducing the shell size by 33% to 4  $\mu\text{m}$  causes the Stokes’ Law Shell velocity to drop to ~0.28 cm/hr, a ~56% decrease. Increasing the temperature from 3.5° C to 6.1° C increases the sinking velocity to 0.70 cm/sec, a 9% increase in sinking velocity. Bach et al. concluded that a 2 degree C temperature increase would result in a 6%

increase in sinking velocity<sup>24</sup>. The two results agree reasonably well. Decreasing the salinity from 34.7 to 33.2 causes the velocity to increase slightly from 0.64 to 0.65 cm/hr, about a 2% increase. Decreasing the size of the Stokes' Law Shell, increasing the temperature, and decreasing the salinity decreases the velocity to 0.29 cm/hr. This is a 55% decrease. The size of the shell has the greatest influence on sinking velocity (Table 7).

Further, the decreased size of a shell will accelerate the rate of dissolution<sup>8</sup> (Equation 7). A shell having a diameter of 6  $\mu\text{m}$  will have a dissolution rate of 3408 %/day. A shell having a diameter of 4  $\mu\text{m}$  will have a dissolution rate of 5462 %/day. The smaller shell has a 60% faster dissolution rate.

Taken together, the slower sinking velocity and the faster dissolution rate will decrease  $\text{CaCO}_3$  transport efficiency by  $\sim 115\%$  (Fig. 3; Equation 8), and thicken the  $\text{CaCO}_3$  transition zone. If the production of surface ocean  $\text{CaCO}_3$  does not increase, or if it decreases, the depth of the CCrD may decrease. The resulting increase in unsaturated water may dissolve  $\text{CaCO}_3$  sediments that are in or below the  $\text{CaCO}_3$  transition zone over long time scales.

In summary, the increase in transport efficiency of  $\text{CaCO}_3$  shells formed the “glacial express” during the LGM. In the future, the expected decrease in  $\text{CaCO}_3$  shell transport efficiency may form an antithetical “canicular local.”

## Discussion

The glacial express hypothesis is based on first-order approximations. This section explores the robustness and limitations of these approximations.

### *Stokes' Law Shells and coccospheres*

Stokes' Law Shells are perfect spheres. The polyhedron shape of coccospheres resembles spheres. To test the validity of using Stokes' Law to approximate sinking rates, I compared how changing size influenced sinking rate for Stokes' Law Shells with how changing size influenced the sinking rates for shells produced by coccolithophores and forams. Monteiro et al. measured the sinking velocity of coccospheres produced by *E. Huxleyi* and *G. Oceanica* grown in the lab<sup>6</sup>. Their experiments were performed at 19° C in artificial sea water. Using their regression line to calculate sinking velocity, a coccosphere with a 6- $\mu\text{m}$  diameter would have an average sinking velocity of 0.325 meters/day (1.35 cm/hour), while coccospheres with 8- $\mu\text{m}$  diameters (i.e., 33% larger) would have an average sinking velocity of 0.825 meters/day (3.44 cm/hour). A 33% increase in size resulted in a 154% increase in sinking velocity, much higher than the  $\sim 62\%$  increase found for Stokes' Law Shells. In short, using Stokes' Law produces a conservative estimate of changes in sinking velocity due to changes in coccolithosphere size.

### *Stokes' Law Shells and foram shells*

Forams also contribute  $\text{CaCO}_3$  to the deep ocean<sup>3</sup>. Berger and Piper<sup>7</sup> measured the settling velocity of foram shells in demineralized water at a temperature of 25° C. The warm temperature and lack of dissolved compounds sped the sinking rate compared to typical seawater. Table 8 shows Berger and Piper's results. Sinking velocities increase with increasing shell size. However, this increase is not linear. Increasing the size of larger shells has a smaller influence on velocity than increasing the size of smaller shells. For example, increasing the shell

size from 125 to 177  $\mu\text{m}$  (42% increase) resulted in a 108% increase in sinking velocity. Increasing the shell size from 177 to 250  $\mu\text{m}$  (41% increase) resulted in a 78% increase in sinking velocity. Extrapolating their results for a 33% size increase leads to a ~63 to ~85% increase in sinking velocity, nearly equal to or slightly more than the velocity increase predicted by Stokes' Law (~62%).

In summary, using Stokes' Law to estimate the increase in sinking velocity due to a size increase underestimates observed changes in sinking velocities due to increasing shell size for both coccospheres and forams. Stokes' Law estimates a ~62% decrease, while coccospheres sank 154% faster and forams sank 63 to 85% faster. Estimates based on Stokes' Law will underestimate increases in  $\text{CaCO}_3$  transport efficiency and require a slightly larger decrease in  $\text{CaCO}_3$  productivity. This increase can be accommodated by the silica hypothesis.

### **Conclusion**

During glacial times,  $\text{CaCO}_3$  shells were larger than their interglacial counterparts<sup>1-5</sup>. This research explores how these larger shells changed geochemical cycles. For example, larger shells help explain why  $\text{CO}_2$  levels were lower, why atmospheric radiocarbon levels were higher, and why the  $\text{CaCO}_3$  transition zone was thinner during glacial times. Larger shells increased  $\text{CaCO}_3$  transport efficiency to the deep ocean by ~90%. Since the delivery of  $\text{CaCO}_3$  to deep-marine sediments was similar between glacial and interglacial times, one expects the production of  $\text{CaCO}_3$  in the surface ocean to have dropped by ~45%. An increase in diatom abundance could have decreased coccolithophore abundance enough to explain the ~45% drop in  $\text{CaCO}_3$  production. Decreasing  $\text{CaCO}_3$  production in the surface ocean would help explain why atmospheric  $\text{CO}_2$  levels were lower during glacial times and why atmospheric radiocarbon levels were higher during glacial times. Increasing the efficiency of  $\text{CaCO}_3$  transport during glacial times would decrease the width of the  $\text{CaCO}_3$  transition zone, while a decrease in  $\text{CaCO}_3$  transport efficiency during interglacial times would increase the width of the  $\text{CaCO}_3$  transition zone. Farrell and Prell observed that the average thickness of the  $\text{CaCO}_3$  transition zone was 230 meters during glacial times and 650 meters during interglacial times<sup>12</sup>, which supports the "glacial express" hypothesis.

1. Beaufort, L. et al. Sensitivity of coccolithophores to carbonate chemistry and ocean acidification. *Nature* **476**, 80-83 (2011).
2. Henderiks, J. & Renaud, S. Coccolith size increase of *Calcidiscus leptoporus* offshore Morocco during the Last Glacial Maximum: an expression of enhanced glacial productivity? *J. Nanoplankton Res.* **26**, 1-12 (2004).
3. Schmidt, D. N., Lazarus, D., Young, J. R. & Kucera, M. Biogeography and evolution of body size in marine plankton. *Earth-Science Reviews* **78**, 239-266 (2006).
4. Barker, S. & Elderfield, H. Foraminiferal calcification response to glacial-interglacial changes in atmospheric CO<sub>2</sub>. *Science* **297**, 833-836 (2002).
5. Moy, A. D., Howard, W. R., Bray, S. G. & Trull, T. W. Reduced calcification in modern Southern Ocean planktonic foraminifera. *Nature Geoscience*. doi: 10.1038/NGEO460 (2009).
6. Monteiro, F. et al. Why marine phytoplankton calcify. *Sci. Adv.* **2**. doi:10.1126/sciadv.1501822 (2016).
7. Berger, W. H. & Piper, D. J. W. Planktonic foraminifera: differential settling, dissolution, and redeposition. *Limnol. Oceanogr.* **17**, 275-287 (1972).
8. Keir, R. S. The dissolution kinetics of biogenic calcium carbonates in seawater. *Geochimica et Cosmochimica Acta* **44**, 241-252, (1980).
9. Kohfeld, K. E., Quéré, C. L., Harrison, S. P. & Anderson, R. F. Role of marine biology in glacial-interglacial CO<sub>2</sub> cycles. *Science* **308**, 74-78 (2005).
10. Catubig, N. R. et al. Global deep-sea burial rate of calcium carbonate during the last glacial maximum. *Paleoceanography* **13**, 298-310 (1998).
11. Anderson, D. M. & Archer, D. Glacial-interglacial stability of ocean pH inferred from foraminifer dissolution rates. *Nature* **416**, 70-73 (2002).
12. Farrell, J.W. & Prell, W.L. Climatic change and CaCO<sub>3</sub> preservation: an 800,000 year bathymetric reconstruction from the central equatorial Pacific Ocean. *Paleoceanography* **4**, 447-466 (1989).
13. Klaas, C. & Archer, D.E. Association of sinking organic matter with various types of mineral ballast in the deep sea: implications for the rain ratio. *Global Biogeochemical Cycles* **16**, 1116. doi:10.1029/2001GB001765 (2002).
14. Feely, R. A. et al. Impact of anthropogenic CO<sub>2</sub> on the CaCO<sub>3</sub> system in the oceans. *Science* **305**, 362-366, (2004).

15. Fabry, V. J., Seibel, B. A., Feely, R. A. & Orr, J. C. Impacts of ocean acidification on marine fauna and ecosystem processes. *ICES J. of Mar. Sci.* **65**, 414-432 (2008).
16. Akester, R. J & Martel, A. L. Shell shape, dysodont tooth morphology, and hinge-ligament thickness in the bay mussel *Mytilus trossulus* correlate with wave exposure. *Canadian Journal of Zoology* **78**, 240-253 (2000).
17. Smith, H. E., et al. Predominance of heavily calcified coccolithophores at low CaCO<sub>3</sub> saturation during winter in the Bay of Biscay. *PNAS* **109**, 8845-8849 (2012).
18. Ramisch, F., Dittrich, M., Mattenberger, C. Wehrli, B. & Wüest, A. Calcite dissolution in two deep eutrophic lakes. *Geochimica et Cosmochimica Acta* **63**, 3349-3356 (1999).
19. Stanley, E. M. & Batten, R.C. Viscosity of sea water at moderate temperatures and pressures. *JGR* **74**, 3415-3420 (1969).
20. Sharqawy, M. H., Lienhard, J. H. & Zubair, S. M. Thermophysical properties of seawater: a review of existing correlations and data. *Desalination and Water Treatment* **16**, 354-380 (2010).
21. Bereiter, B., Shackleton, S., Baggenstos, D., Kawamura, K., & Severinghaus, J. Mean global ocean temperatures during the last glacial transition. *Nature* **553**, 39-44 (2018).
22. Adkins, J. F., McIntyre, K. & Schrag, D. P. Salinity, temperature and  $\delta^{18}\text{O}$  of the glacial deep ocean. *Science* **298**, 1769-1773 (2002).
23. Paasche, E. A review of the coccolithophorid *Emiliana huxleyi* (Prymnesiophyceae), with particular reference to growth, coccolith formation, and calcification-photosynthesis interactions. *Phycologia* **40**, 503-529 (2002).
24. Bach, L.T. et al. An approach for particle sinking velocity measurements in the 3-400  $\mu\text{m}$  size range and considerations on the effect of temperature on sinking rates, *Mar. Biol.* **159**, 1853-1854 (2012).
25. Morse, J. W. Dissolution kinetics of calcium carbonate in sea-water: VI. the near-equilibrium dissolution kinetics of calcium carbonate-rich sediments. *Am. J. Sci.* **278**, 344-353 (1978).
26. Archer, D. & Maier-Reimer, E. Effect of deep-sea sedimentary calcite preservation on atmospheric CO<sub>2</sub> concentration. *Nature* **367**, 260-263 (1994).
27. Hughen, K. et al. <sup>14</sup>C activity and global carbon cycle changes over the past 50,000 years. *Science* **303**, 202-207 (2004).
28. Harrison, K.G. Role of increased silica input on paleo-CO<sub>2</sub> levels. *EOS* **76**, 46 (1995).
29. Harrison, K.G. Role of increased marine silica input on paleo-pCO<sub>2</sub> levels. *Paleoceanography* **15**, 292-298 (2000).

30. Matsumoto, K., Sarmiento, J. L. & Brzezinski, M. A. Silicic acid leakage from the Southern Ocean: a possible explanation for glacial atmospheric pCO<sub>2</sub>, *Global Biogeochem. Cycles* **16**, 1031. doi:10.1029/2001GB001442 (2002).
31. Hutchins, D.A. & Bruland, K.W. Iron-limited diatom growth and Si:N uptake ratios in a coastal upwelling regime. *Nature* **393**, 561-564 (1998).
32. Takeda, S. Influence of iron availability on nutrient consumption ratio of diatoms in oceanic waters. *Nature* **393**, 774-777 (1998).
33. Brzezinski, M.A., Dumousseaud, C., Krause, J.W., Measures, C.I. & Nelson, D.M. Iron and silicic acid concentrations together regulate Si uptake in the equatorial Pacific Ocean. *Limnol. Oceanog.* **53**, 875-889 (2008).

**Acknowledgements** I thank BAZ, EGS, RT, RM and WH. This research would not have been possible without the foresight of Lieutenant Matthew Fontaine Maury and Drs. Keir, Farrell, and Prell. This research did not involve funding.

**Author contributions** Kevin Harrison wrote the paper.

**Competing Interests** The author has no competing interests.

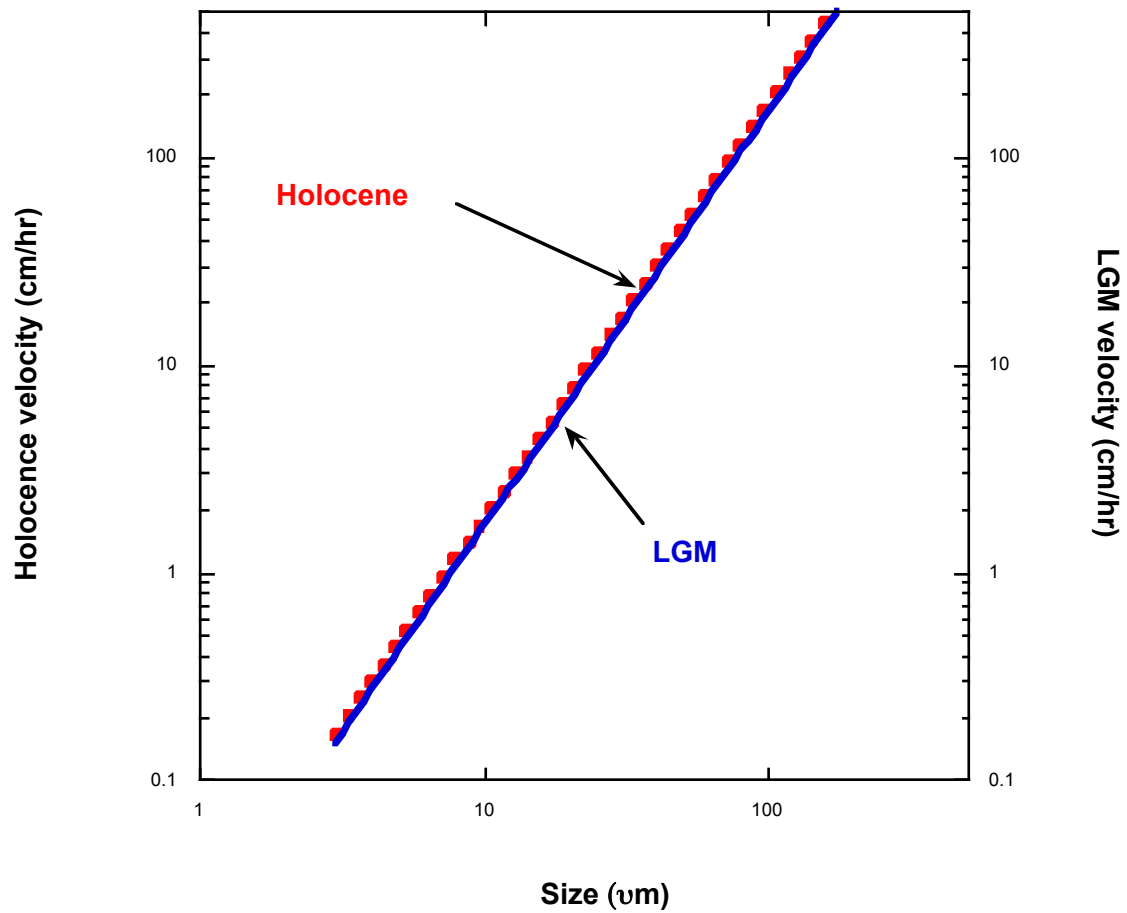


**Fig. 1 | Stokes' Law velocity estimates vs. particle size.** Stokes' Law velocities were calculated for Holocene and LGM conditions (Equation 4). For a given particle size, a Stokes' Law particle will sink slightly faster during the Holocene than during the LGM, because LGM seawater is more dense and has a higher dynamic viscosity (Table 4).

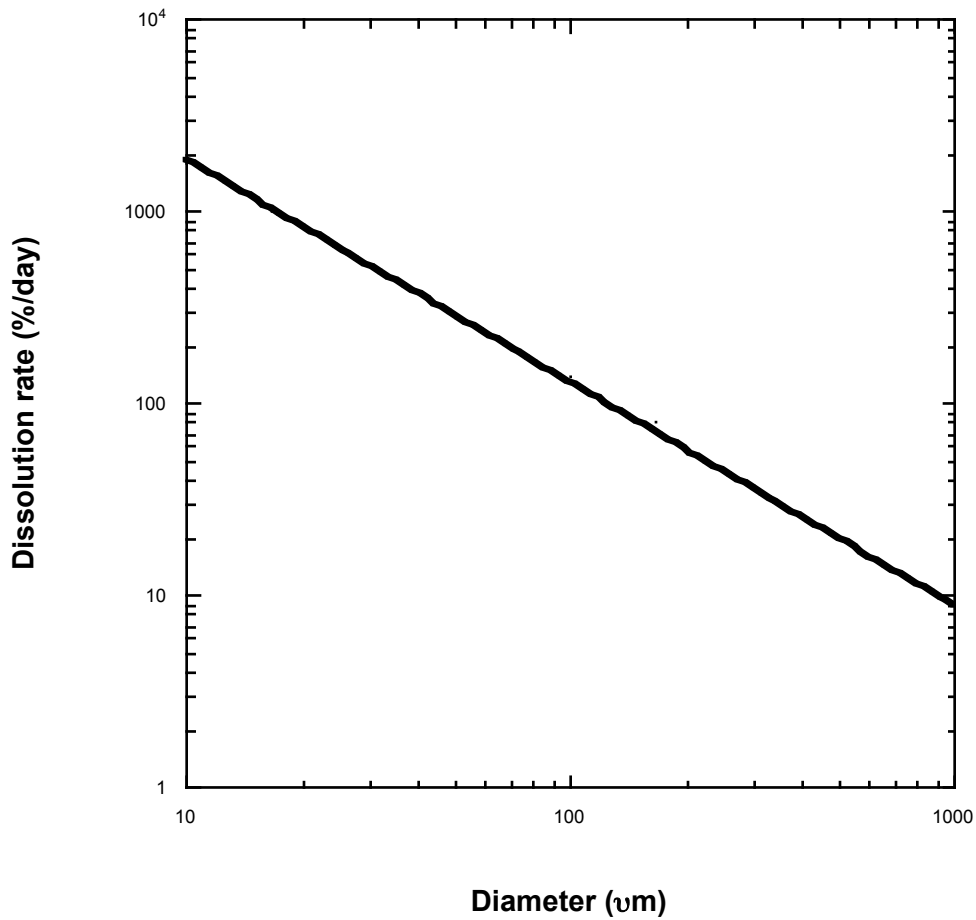


**Fig. 2 | Diameter vs. Dissolution rate.** As diameter increases, dissolution rate decreases. This figure is based on the work of Keir<sup>8</sup> and Equation 7. Lower pCO<sub>2</sub> levels and high-energy environments may increase shell diameter.



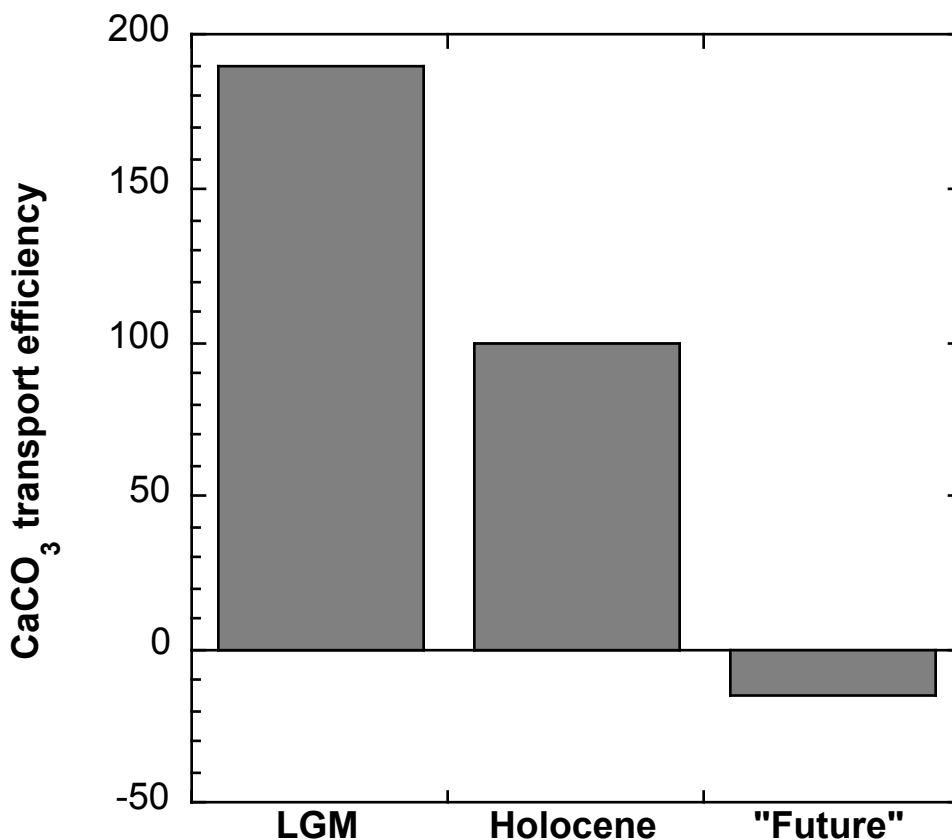


**Fig. 3 | CaCO<sub>3</sub> transport efficiency: LGM, Holocene, and “Future.”** CaCO<sub>3</sub> transport efficiency is calculated by subtracting the velocity change from the dissolution rate change (Equation 8). Holocene CaCO<sub>3</sub> transport efficiency is normalized to 100%. During the LGM, the ocean was ~2.6° C cooler, the salinity was ~1.2‰ greater, and CaCO<sub>3</sub> shells were ~33% larger. LGM CaCO<sub>3</sub> transport was 90% more efficient than in the Holocene (i.e., CaCO<sub>3</sub> shells took the “glacial express”). In the “Future” scenario, the ocean may be ~2.6° C warmer, the salinity may be ~1.2‰ less, with CaCO<sub>3</sub> shells ~33% smaller. Based on past trends, “Future” CaCO<sub>3</sub> transport may be 115% less efficient than in the Holocene (i.e., CaCO<sub>3</sub> shells may take the antithetical “canicular local”).

**Table 1 | Glacial/Interglacial CaCO<sub>3</sub> shell differences**

---

Species	Last Glacial Max.	Holocene	% Difference	Reference
<b>Coccolithophores:</b>				
Average coccolith mass	12 pg	9 pg	33%	(1)
<i>E. Huxleyi</i> coccolith mass	5.2 pg	4.3 pg	21%	(1)
<i>G. Oceanica</i> coccolith mass	24.5 pg	21 pg	17%	(1)
<i>C. Leptoporus</i> coccolith size pelagic low energy	7.47±0.05 μm	6.65±0.36 μm	12%	(2)
<b>Forams:</b>				
<i>G. Bulloides</i> size fraction, core NEAP 8K Foram mass	18 μg	12 μg	50%	(4)
<i>G. Bulloides</i> Foram mass	30.3 μg	24.4 μg	24%	(5)

---

**Table 2 | Glacial/Interglacial coccolith differences in high-energy and low-energy environments**

Climate	Low energy: core	size ( $\mu\text{m}$ )	High energy: core	size ( $\mu\text{m}$ )
LGM	4242-93	7.43 $\pm$ 1.79	5559-48	8.86 $\pm$ 1.77
	4241-43	7.50 $\pm$ 1.52	4216-02	8.27 $\pm$ 1.51
			1048-78	7.22 $\pm$ 1.65
	<b>Average</b>	<b>7.47<math>\pm</math>0.05</b>	<b>Average</b>	<b>8.12<math>\pm</math>0.83</b>
Holocene	N3KF21	6.92 $\pm$ 1.36	5559-48	7.28 $\pm$ 1.48
	T88-9P	6.24 $\pm$ 1.02	4216-02	7.35 $\pm$ 1.31
	4242-01	6.78 $\pm$ 1.05	V23-98	7.25 $\pm$ 1.55
	<b>Average</b>	<b>6.65<math>\pm</math>0.36</b>	<b>Average</b>	<b>7.29<math>\pm</math>0.05</b>

Low-energy Holocene coccoliths are the smallest, while high-energy LGM coccoliths are the largest. Low-energy LGM coccoliths are slightly larger than high-energy Holocene coccoliths. High-energy Holocene coccoliths may serve as useful surrogates for low-energy LGM coccoliths in future studies. Data from Henderiks and Renaud's<sup>2</sup> Table 2. Cores were collected from the North Atlantic.

**Table 3 | Gale frequency and heavily-calcified coccolithophore abundance in the Bay of Biscay**

---

Month	# of gales	heavily-calcified coccolith morphotype abundance
January	10	nd
February	10	>90%
March	7	>75%
April	4	~25%
May	2	~10%
June	1	<10%
July	1	<10%
August	1	~20%
September	2	~20%
October	6	~10%
November	9	~50%
December	13	>75%

---

Smith et al. collected *E. Huxleyi* coccolithophores in the Bay of Biscay<sup>17</sup>. They distinguished between typical *E. Huxleyi* and heavily-calcified *E. Huxleyi*. When gales are more frequent, heavily-calcified *E. Huxleyi* morphotypes are more abundant. A gale is Force 8 or greater on the Beaufort Scale. Force 8 corresponds to wind speeds over 62 km/hr and wave heights over 5.5 meters. The data for the number of gales was collected from the Pilot Chart of the North Atlantic Ocean (~1850 to ~2000): (<http://www.offshoreblue.com/navigation/pilot-charts.php>).

**Table 4 | Sinking velocities for Stokes' Law Shells during the Holocene and LGM**

	Holocene	LGM
Shell diameter ( $\mu\text{m}$ )	6	8 (33% increase)
Temperature ( $^{\circ}\text{C}$ )	3.5	0.9
Salinity ( $\text{‰}$ )	34.7	35.85
Shell density (g/ml)	1.2	1.2
<b>Pressure = 1 bar</b>		
Dynamic viscosity (kg/(m*sec))	$1.70 \times 10^{-3}$	$1.85 \times 10^{-3}$
Seawater density (g/ml)	1.028	1.029
Velocity (cm/hr)	0.71	1.16 (64% increase)
<b>Pressure = 200 bar</b>		
Dynamic viscosity (kg/(m*sec))	$1.68 \times 10^{-3}$	$1.82 \times 10^{-3}$
Seawater density (g/ml)	1.037	1.038
Velocity (cm/hr)	0.68	1.12 (65% increase)
<b>Pressure = 400 bar</b>		
Dynamic viscosity (kg/(m*sec))	$1.65 \times 10^{-3}$	$1.80 \times 10^{-3}$
Seawater density (g/ml)	1.046	1.047
Velocity (cm/hr)	0.66	1.07 (62% increase)

Sinking velocities are calculated for three pressures: 1 bar, 200 bar, and 400 bar. One bar roughly corresponds to sea level. 400 bar roughly corresponds to pressure near the  $\text{CaCO}_3$  transition zone. 200 bar falls between the surface and the transition zone. As pressure increases, the sinking velocity decreases slightly, due to increased seawater density. A 33% increase in size causes velocities to increase by at least 62% at every depth.

**Table 5 | Atmospheric CO<sub>2</sub> values: LGM to Holocene**

---

LGM to Holocene	$\Delta\text{CO}_2$	CO <sub>2</sub>	Reference
Observed LGM	--	196	(26)
Terrestrial biosphere increase	-22	174	(9)
Ocean temperature increase	+26	200	(9)
Ocean salinity decrease	-13	187	(9)
CaCO <sub>3</sub> production increase (+45%)	+95	282	See text
Observed interglacial	----	280	(26)

---

During the LGM, the atmospheric CO<sub>2</sub> concentration was 196 ppm. CO<sub>2</sub> values rose to 280 ppm during the Holocene. Models that take into account the increasing size of the terrestrial biosphere, warming oceans, and decreasing ocean salinity would cumulatively lower CO<sub>2</sub> levels to 187 ppm. Predicted increases to surface ocean CaCO<sub>3</sub> production of 45% would increase atmospheric CO<sub>2</sub> levels to 282 ppm, close to the observed interglacial value.

**Table 6 | Atmospheric radiocarbon budget: LGM to Holocene**

LGM to Holocene	Radiocarbon change (‰)	Radiocarbon value (‰)	Reference
Observed LGM	--	+375±25	(27)
Increased terrestrial biosphere mass	-20±10	+330±35	(27)
50% increase in ocean ventilation	-150±50	+180±85	(27)
45% increase in CaCO <sub>3</sub> production	-135	+45±85	See text
Observed Holocene	--	0	(27)

During the LGM, atmospheric radiocarbon values were +375±25‰. These values decreased to 0‰ in the Holocene. Estimates of increased terrestrial biomass, increased ocean ventilation, and a 45% increase in CaCO<sub>3</sub> surface ocean production could decrease atmospheric radiocarbon values to +45±85‰.

**Table 7 | Future “canicular local” CaCO<sub>3</sub> transport by smaller shells in a warmer, less-saline ocean**

	Holocene (from Table 4)	Reduced shell size	Increased Temp.	Decreased Salinity	Combined effect of: Reduced shell size Increased Temp. Decreased Salinity
Shell Diameter ( $\mu\text{m}$ )	6	<b>4</b>	6	6	<b>4</b>
Temp. ( $^{\circ}\text{C}$ )	3.5	3.5	<b>6.1</b>	3.5	<b>6.1</b>
Salinity ( $\text{‰}$ )	34.7	34.7	34.7	<b>33.15</b>	<b>33.15</b>
Shell Density (g/ml)	1.2	1.2	1.2	1.2	1.2
Seawater Density (g/ml)	1.046	1.046	1.045	1.044	1.044
Dynamic Viscosity (kg/m-sec)	$1.65 \times 10^{-3}$	$1.65 \times 10^{-3}$	$1.52 \times 10^{-3}$	$1.64 \times 10^{-3}$	$1.52 \times 10^{-3}$
velocity (cm/hr)	0.64	0.28	0.70	0.65	<b>0.29</b>

Stokes’ Law is used to explore how CaCO<sub>3</sub> sinking velocity may change in the future, as shell size decreases, temperature increases, and salinity decreases. **Bolded** numbers signify the changes. Shell size is decreased by 33%. Temperature is increased by 2.6° C. Salinity is decreased by 1.55‰. These values reflect the magnitude of changes observed during the LGM-to-Holocene transition and are for illustrative purposes. The sinking velocity will decrease from 0.64 to 0.29 cm/hr, a 55% decrease. Most of this decrease is due to the change in particle size, not to temperature or salinity. 400 bar, a pressure near the top of the CaCO<sub>3</sub> transition zone, was used for these calculations.



**Table 8 | Foram settling velocities**

---

Size ( $\mu\text{m}$ )	Velocity (cm/sec) (cm/s)	Max size ( $\mu\text{m}$ )	Size increase	Max Vel. (cm/s)	Velocity increase
62-125	0.24-0.35	125	--	0.35	--
125-177	0.56-0.73	177	42%	0.73	108%
177-250	0.80-1.3	250	41%	1.3	78%
>250					

---

Berger and Piper<sup>7</sup> collected size fractions of forams and measured their sinking velocities in demineralized water at 25° C. The maximum size was picked to be the upper boundary of each size fraction. The percent size increase was calculated from the maximum sizes of each size fraction. The maximum velocity was calculated from the maximum velocities of each size fraction. The observed change in velocity for increased foram size is greater than the theoretical Stokes' Law predictions. Stokes' Law gives a conservative estimate.